



# Hierarchical Nested Wrinkles on Silica–Polymer Hybrid Films: Stimuli-Responsive Micro Periodic Surface Architectures

Yasuaki Tokudome\*, Kazumasa Suzuki, Takuya Kitanaga & Masahide Takahashi\*

Department of Materials Science, Graduate School of Engineering, Osaka Prefecture University, Sakai, Osaka, 599-853, Japan.

SUBJECT AREAS:

POLYMERS AND SOFT MATERIALS

MATERIALS CHEMISTRY

INORGANIC CHEMISTRY

ENGINEERING

Received  
14 June 2012

Accepted  
5 September 2012

Published  
21 September 2012

Correspondence and requests for materials should be addressed to Y. T. (tokudome@photomater.com) or M. T. (masa@photomater.com)

\* These authors contributed equally to this work.

Stimuli-response on hierarchically-structured surface wrinkles is required for advanced filtration, catalysis and sensing applications. Although conventional processes can form hierarchical surface wrinkles, incorporation of stimuli-responsive features has not been achieved, limiting the potential multi-scale functionality of wrinkles. Here, we demonstrate a novel process that can fabricate stimuli-responsive surface hierarchical structures on silica–polymer hybrid films through precisely controlled UV-polymerization and sol-gel condensation. Starting from uniform hybrid films, UV excitation of the film surface triggers the formation of micrometre-scale wrinkles with dual periodicity. Hierarchical nested wrinkle (NW) structures with controllable periodic lengths at discrete size scales of  $< 10 \mu\text{m}$  and  $> 23 \mu\text{m}$  show a shape-memory effect with changes in the surrounding humidity. Moreover, the individual responses of wrinkles with different periodicities can be controlled independently. As a proof-of-concept application, we demonstrate that the NW structures are an active size-selective adsorption/release surface for micrometre-sized particles.

Smart materials, which respond to external stimuli, have been expected to play a significant role in new-generation nano- and microdevices, because of their capabilities as separation media<sup>1,2</sup>, actuators<sup>3,4</sup>, host materials for drug delivery<sup>5,6</sup>, and so on. As well as many studies into stimuli-responsive organic polymers, tremendous effort has been devoted to the fabrication of stimuli-responsive organic/inorganic materials. Owing to the relatively high chemical and physical durability provided by an inorganic moiety, organic/inorganic materials are promising candidates for nano- and microdevices<sup>7</sup>. However, the stimuli-responses in those hybrid materials are in fact usually brought about by active organic moieties that are less durable than the associated inorganic frameworks. Thus, the development of versatile, durable, active materials is still one of central issues in materials science.

As an approach to stimuli-response in organic/inorganic systems, we focus here on the formation of surface wrinkles. Surface wrinkle formation is a well-known physical process observed in nature; an example of such responsive wrinkles is the skin of animals, where wrinkles form and vanish depending on the movement of the muscles underneath. The versatility of the process has been demonstrated<sup>8–15</sup> for diverse materials, revealing that wrinkle formation takes place in a multilayered film comprising a stiff cover layer on a relatively soft, elastic substrate. Bowden *et al.* first reported that surface wrinkling can be induced in poly(dimethylsiloxane) (PDMS) based films with multilayered structures, such as metal–PDMS<sup>8</sup> and SiO<sub>2</sub>–PDMS<sup>9</sup>. Stress-driven instability initiated at the interface between the layers results in buckling with a periodicity typically in the micrometre regime<sup>12,13</sup>. The ability to form surface wrinkles was demonstrated to be a general feature of metal–organic multilayered systems<sup>10</sup>. The mechanism for forming surface wrinkles<sup>16–18</sup> should also be applicable to organic/inorganic hybrid systems without active organic molecules.

Since the wrinkle formation process only depends on the generation of a stress mismatch between two adjacent layers, a variety of materials can be chosen depending upon the application. Moreover, when the stress mismatch can be controlled by external stimuli, hybrid materials with stimuli-responsive microstructures should be attained without incorporation of any active organic moieties. Indeed, the formation of such active wrinkles has previously been reported for surface-treated PDMS<sup>19</sup> and titania-polymer hybrid films<sup>20,21</sup>. However, the periodicities of these active surface wrinkles were over  $10 \mu\text{m}$ , which is unsuitable for nanoscale applications. Besides, the formation of hierarchical nested wrinkle (NW) structures with an active surface has not been reported. Such a

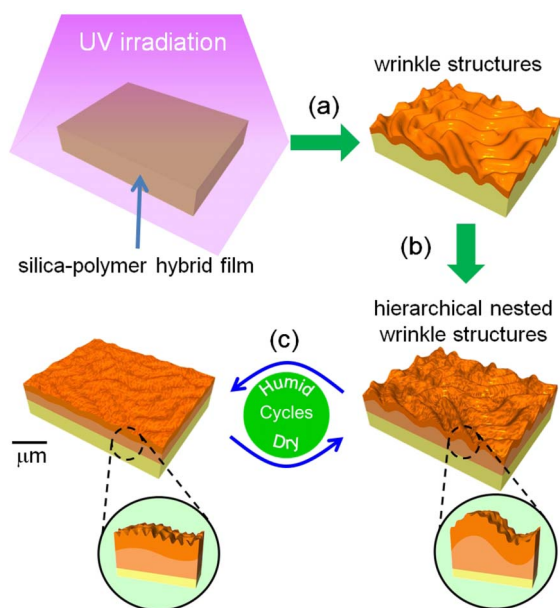


**Figure 1** | A strategy for stimuli-responsive hierarchical NW structures. (a) UV irradiation on the surface of a silica–photomonomer hybrid film drives photopolymerization and condensation reactions, leading to surface wrinkle formation. (b) Adjustment of the film thickness can create hierarchical nested wrinkle structures. The periodicity of the smallest wrinkles is 4.9 μm. (c) obtained hierarchical wrinkle structures are humidity responsive, and the responses of wrinkles of different generations can be controlled independently.

combination would exploit the potential multi-scale functionality of wrinkles. Therefore, the combination of stimuli-response and individual control of structures on discrete size scales is of great interest and is yet to be realized.

Here, we present three main findings which overcome the previously mentioned limitations regarding wrinkle formation: (1) achievement of stimuli-responsive hierarchical surface wrinkles with controlled periodicity ranging from a few to several tens of micrometres; (2) fabrication of active surface wrinkles with the periodicities of < 10 μm; (3) control of the individual stimuli-responses of wrinkles with different size scales. The wrinkle structures were readily formed on the surface of uniform silica–polymer hybrid films by surface-limited UV excitation (Fig. 1a). The periodicity of the NW structures can be independently controlled for different generations of wrinkles (we obtained periodicities of a few μm and several tens of μm; the periodic length of the smaller wrinkles was well below 10 μm

(Fig. 1b). Humidity change was adopted as the external stimulus in this study, and independent control of wrinkle structures with different periodicities was achieved (Fig. 1c).

Because the method used in this study is very versatile, the NW structures presented open up further opportunities for applications such as controlled release or capture of particles with different sizes<sup>19,22</sup>, by tailoring the responses from the individual size scales. As a proof-of-concept application, size-selective adsorption of particles from polydispersed colloids has been successfully demonstrated.

## Results

**Nested wrinkle formation on silica-polymer hybrid films.** Nested wrinkle formation has been demonstrated in a silica–polymer hybrid system, tetraethoxysilane (TEOS) and acrylamide (AM), also containing poly(vinylpyrrolidone) (PVP). Condensation of hydrolyzed-TEOS and UV-photopolymerization of AM were induced simultaneously in a uniform spin-coated film by simple UV exposure. The penetration of the UV into the film surface was controlled so that a bilayer structure with wrinkles was formed (Supplementary Fig. S1). Fourier transform infrared (FT-IR) measurements on the surface and substrate sides of the film revealed that most of the poly(acrylamide) (PAM) is in the surface layer, whereas PVP and silica, together with residual AM, are predominantly located in the bottom layer (Supplementary Fig. S2). Figure 2 shows laser scanning confocal microscopy (LSCM) images of the films spin-coated at various spinning rates. The morphology clearly changes with spinning rate, *i.e.* film thickness, *t*. Wrinkles with a periodic length,  $\lambda$ , of 22.6 μm are formed on a film deposited at a spinning rate of 2000 rpm ( $t \sim 7.9 \mu\text{m}$ ), where no other periodic structure is observed (Fig. 2a). On the other hand, NW structures are formed on films deposited at spinning rates of 1500 rpm ( $t \sim 9.5 \mu\text{m}$ ) and 1000 rpm ( $t \sim 12.4 \mu\text{m}$ ). We hereafter call these wrinkles with smaller and larger periodicities the “1G structure” (the 1<sup>st</sup> generation structure) and “2G structure” (the 2<sup>nd</sup> generation structure), respectively. At a spinning rate of 1000 rpm ( $t \sim 12.4 \mu\text{m}$ ),  $\lambda$  values of 1G and 2G structures are 7.0 and 29.2 μm, respectively (Fig. 2b). For spinning rates below 750 rpm ( $t \sim 16.6 \mu\text{m}$ ), 1G structures dominate, and are accompanied by 2G structures of  $\sim 50 \mu\text{m}$  in periodicity. At a spinning rate of 500 rpm ( $t \sim 23.1 \mu\text{m}$ ), the 1G structure shows  $\lambda = 10.1 \mu\text{m}$ , whereas the minor 2G structure shows  $\lambda = 75.2 \mu\text{m}$  (Fig. 2c). The 2G structure forms only minor domains and is barely observed at the magnification used in the figure.

**Detailed analyses of nested wrinkle structures.** Cross-sectional observation of the fractured surface of a NW structure (spinning rate: 1000 rpm) reveals that the film is composed of three layers (Fig. 3a). These layers will be referred to as layer 1 (closest to the

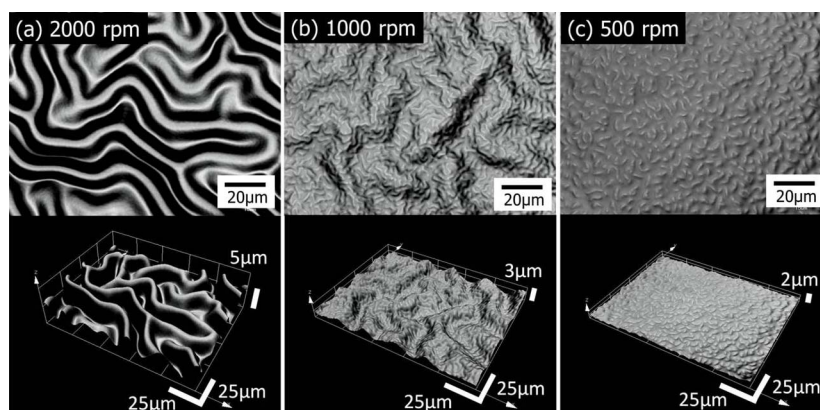


**Figure 2** | 3D images of wrinkles with various structures and periodicities. Top-view and tilt-view images of films coated on a glass substrate at spinning rates of (a) 2000 rpm, (b) 1000 rpm, and (c) 500 rpm. The images were obtained by stacking two-dimensional optically sliced LSCM images.

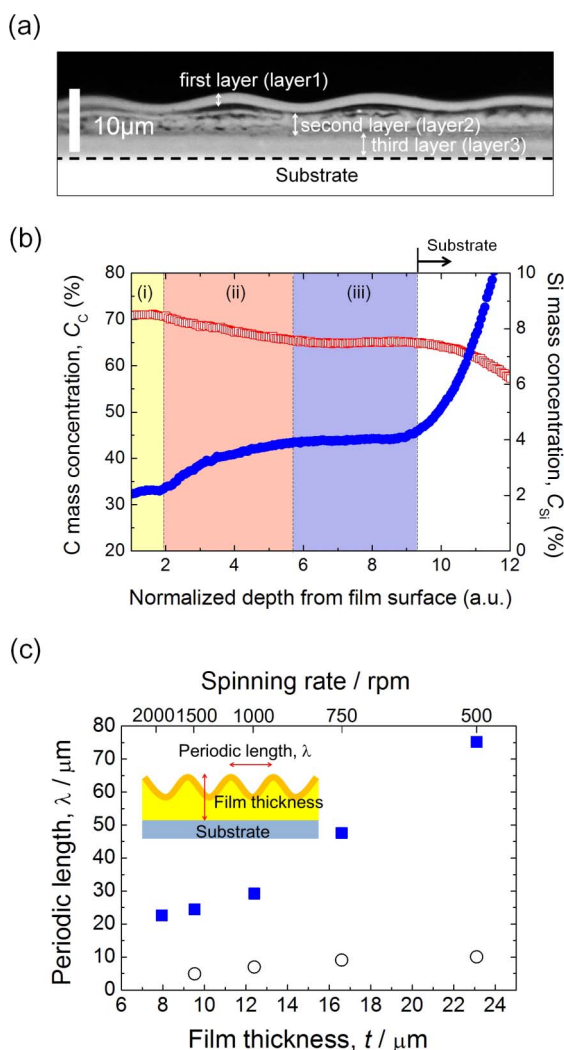


**Figure 3** | Detailed analyses of NW structures. (a) cross-sectional optical microscope image of a fractured surface of the NW structure prepared on a Si substrate at 1000 rpm. The black dotted line indicates the substrate/layer 3 interface. (b) depth profiles of atomic mass concentrations in a trilayer film analyzed by GD-OES;  $\square$  (red): C ( $C_C$ );  $\bullet$  (blue): Si ( $C_{Si}$ ). The three regimes (i), (ii), and (iii) correspond to layers 1, 2 and 3 in (a), respectively. A steep increase in  $C_{Si}$  at the inside part of the film is because the sputtering has penetrated the film and reached the Si substrate. (c) Dependence of periodic length of wrinkle structures on total film thickness;  $\blacksquare$  (blue): 2G structure;  $\circ$ : 1G structure. Corresponding spinning rates for the respective film thicknesses are given on the upper axis. The analysis was performed using 2D LCSM images. Periodic length,  $\lambda$ , the in-plane periodic length of the wrinkles, was estimated by two-dimensional Fourier transformation of the images. For spinning rates of 750 and 500 rpm,  $\lambda$  values of the 1G and 2G structures were evaluated for respective domains. The coatings were made on a glass substrate.

film surface), layer 2, and layer 3 (closest to the substrate). On this image, a wavy 2G structure is confirmed on the film surface, but the amplitude of the 1G structure is too small to be apparent at this magnification. Taking into account the FT-IR results of Supplementary Fig. S2, layer 1 and layer 3 are considered to be PAM and silica-PVP layers, respectively. Glow-discharge optical emission spectroscopy (GD-OES) was performed on the film with NW structure to evaluate depth profiles of atomic mass concentrations through the film. Figure 3b shows the depth profiles of C and Si ( $C_C$  and  $C_{Si}$ ) for the trilayer film.  $C_C$  decreases with distance from the film surface, whilst  $C_{Si}$  increases. Both  $C_C$  and  $C_{Si}$  show plateaus in the

regimes labelled (i) and (iii). Regime (i) with high  $C_C$  and low  $C_{Si}$  convincingly corresponds to layer 1. On the other hand, regime (iii) with relatively lower  $C_C$  and higher  $C_{Si}$  can be ascribed to layer 3. The C/Si mass ratios at regime (i) and regime (iii) are 32.6 and 16.0, respectively. The value of 16.0 is comparable to the nominal C/Si ratio of 13.9 calculated from the starting composition (See Supplementary Note S1), which is further evidence that the bottom layer is composed of PVP and silica, with some residual AM and photoinitiator, 4,4'-Bis(dimethylamino)benzophenone (BDBP). The gradual decrease of  $C_C$  and increase of  $C_{Si}$  in regime (ii) indicates the formation of a diffusive layer between (i) and (iii).

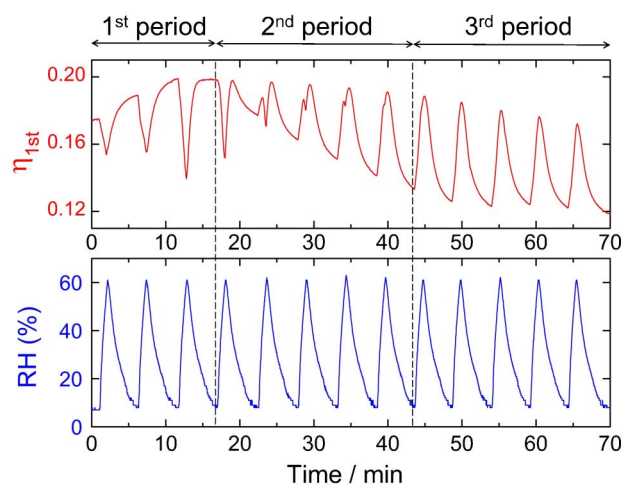
*In situ* observation of the NW formation process was performed to directly observe the kinetics of wrinkle formation. Supplementary Fig. S3 shows the time evolution of NW formation. No structure was observed for the first 2 hours of UV illumination (Supplementary Fig. S3a). After 147 min of illumination, wrinkles of 1G structure appeared gradually (Supplementary Fig. S3b). 7 min later, additional wrinkles of 2G structure started to form (Supplementary Fig. S3c), and the amplitude of the wrinkles increased progressively (Supplementary Fig. S3d–f).

Figure 3c shows the relationship between the periodic length,  $\lambda$ , and the film thickness,  $t$ . The values of  $\lambda$ , spanning from a few to several tens of micrometres, can be tuned with  $t$ . Since the evaporation of solvent is retarded with increasing film thickness, the condensation of hydrolyzed-TEOS becomes correspondingly slower. Indeed, the time required for wrinkle formation depends on the film thickness:  $\sim 1.5$  h for  $t \sim 7.9$  μm (2000 rpm) and almost 4 h for  $t \sim 23.1$  μm (500 rpm). The thicker film will have a thicker PAM layer, as a result of the longer reaction time under UV irradiation. Also, the decreased spinning rate leads to an increase in the net amount of AM on a substrate, which ensures the formation of a thick PAM layer. According to the well-known scaling law,  $\lambda$  increases with increasing thickness of the stiff upper layer<sup>17,23</sup>. The larger  $\lambda$  with increasing film thickness can thus be generally ascribed to the increased PAM layer thickness, though the successive formation of 1G and 2G structures would result in some deviation from the scaling law developed for wrinkles with single periodicity.

### Stimuli-responsive nested wrinkles under humidity modulation.

The NW structures thus obtained are comprised of multilayers with different hydrophobicities: a relatively hydrophobic PAM layer (layer 1), intermediate layer (layer 2), and hydrophilic silica-PVP composite layer (layer 3). Thus, the exposure of the film to moisture can lead to selective swelling of the bottom hydrophilic layers. The selective swelling of the bottom layers affords stress accumulation and/or stress release at the heterointerface, and hence, a change in the wrinkle morphology with changing humidity.

To demonstrate the humidity response of NW structures, *in situ* small angle light scattering (SALS) measurements were carried out on a film coated at 1000 rpm ( $t \sim 12.4$  μm). When the samples show wrinkles on their surfaces, they act as “Bragg gratings” against incident laser light, because of the regular spacing between the wrinkles<sup>24</sup>. The more corrugated the surface, the higher the resultant diffraction efficiency. In the present setup, the light scattered by the 1G structure would be beyond the range of our detector. Thus, the SALS analysis in this study focused on changes in the 2G structure of the NW structures. Figure 4 shows the relationship between relative humidity (RH) and 1<sup>st</sup> order diffraction efficiency ( $\eta_{1st}$ ).  $\eta_{1st}$  is negatively-correlated with RH until the 3<sup>rd</sup> cycle (1<sup>st</sup> period in Figure 4);  $\eta_{1st}$  decreases and increases as RH increases and decreases, respectively. From the 4<sup>th</sup> to 8<sup>th</sup> cycle,  $\eta_{1st}$  shows a much more complicated response to RH change, with additional positive correlations observed (the 2<sup>nd</sup> period in Figure 4). Beyond the 9<sup>th</sup> cycle,  $\eta_{1st}$  only shows positive correlation with RH (3<sup>rd</sup> period in Figure 4);  $\eta_{1st}$  increases and decreases as RH increases and decreases, respectively.



**Figure 4 | Demonstration of humidity response of NW structures.** Change in the 1<sup>st</sup> order diffraction efficiency with humidity cycling, measured on a film with NW structure. The 1<sup>st</sup> order diffraction efficiency ( $\eta_{1st}$ ) = (intensity of the first order diffraction ring)/(intensity of the incident laser light). The measurement was performed on a film coated at a spinning rate of 1000 rpm ( $t \sim 12.4 \mu\text{m}$ ) onto a glass substrate.

It should be pointed out that the present silica–polymer hybrid film shows humidity response even in the low RH range, below 60% (in other words, the ambient humidity range of daily life), with the sensitivity of the response, *i.e.*, the amplitude of the change in  $\eta_{1st}$  with RH change, remaining constant even after 50 cycles. In the 1<sup>st</sup> period, increased humidity induces swelling of layer 3, the bottom hydrophilic layer comprised of silica–PVP, leading to the disappearance of the wrinkles and the decrease in  $\eta_{1st}$ . The swollen bottom layer contracts again with decreasing humidity, resulting in the increase in  $\eta_{1st}$ . On the other hand, the appearance of an additional positive response in the 2<sup>nd</sup> period and the positive correlation in the 3<sup>rd</sup> period suggest that a different type of humidity response has started to occur with subsequent humidity cycles. The humidity response that arises with increased cycling involves the formation of microcracks. Large curvature at the top of the wrinkles can induce fracture of the stiff top layer and formation of microcracks. Since the width of the microcracks alters with swelling of the underlying layer,

the film now shows a positively-correlated humidity response; where the width of the microcracks increases and decreases as the underlying bottom layers swell and shrink, respectively. Indeed, a comparison of the film before and after the SALS measurements (Fig. 5 a, b) reveals that microcracks which reflect the original periodic length of the wrinkles were formed during the course of the repeated RH modulation. The 2G structure with large curvature disappears, and an alternative stress-released flat surface forms, because of the microcrack generation, leading to the positive correlation with RH. The response of the microcracks to decreasing RH is an example of so-called “self-healing” behaviour, accompanied by the recovery of the “wounds” on the film. A schematic illustration of the humidity response of the 2G structure is presented in Fig. 5c. It is noteworthy that the 1G structure is free from microcracking (Fig. 5 d, e). The humidity response of the 1G structure has been qualitatively confirmed as shown in Fig. 5 f, g. Wrinkles disappear at higher humidity, and recover at lower humidity (which is the expected behaviour in the wrinkle regime).

**Selective adsorption of micrometre-sized particles.** Finally, we demonstrate that the NW structures are effective as size-selective adsorption surfaces for micrometre-sized particles (see Supplementary Method S1). As shown in Fig. 6a and Supplementary Fig. S4, polydispersed polystyrene (PS) particles are selectively captured by wrinkles. 1G and 2G structures are effective as a size-selective adsorption surface for micrometre-sized particles, leading to adsorption of a specific particle size distribution (Fig. 6b). It should be noted here that particles over 8  $\mu\text{m}$  diameter are completely excluded (*i.e.* not adsorbed). The 1G-dominated structure (Sieve-1) preferentially selects 2–4  $\mu\text{m}$  particles, whereas nested wrinkle structures (Sieve-2 and Sieve-3) accept up to  $\sim 8 \mu\text{m}$  particles due to the additional contribution from the 2G structure. Decreased spinning rate increases the  $\lambda$  values of both 1G and 2G structures, and therefore, Sieve-2 retains larger particles than those retained by Sieve-3; Sieve-2 adsorbs more 2–4 and 6–8  $\mu\text{m}$  particles and fewer 0–2 and 4–6  $\mu\text{m}$  particles.

## Discussion

The wrinkle formation demonstrated in this study is induced by concurrent chemical bond-forming reactions, rather than by previously reported triggers, such as surface oxidation<sup>9</sup>, sputtering deposition<sup>8</sup>, or gradient polymerization<sup>14,15</sup>. The newly-designed reaction

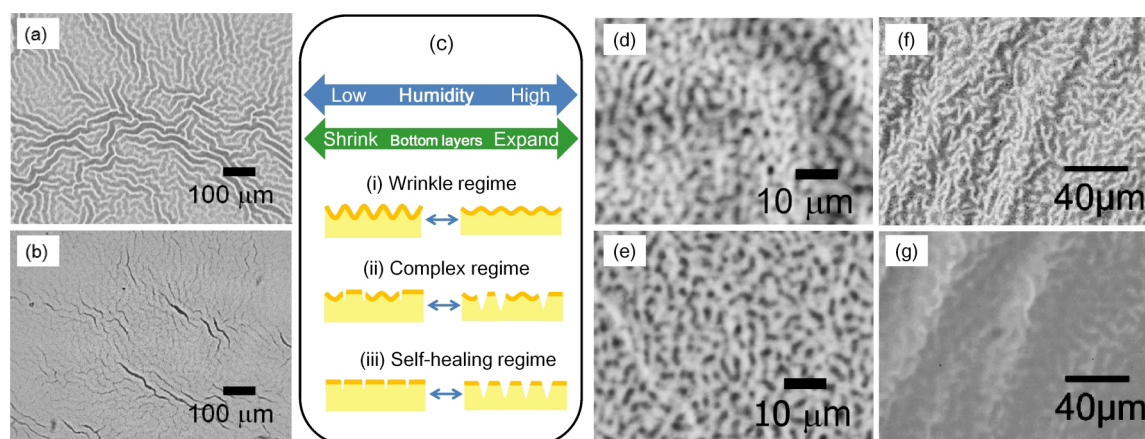


**Figure 5 | Stimuli responses from different wrinkle structures with distinct size scales.** Optical microscope images of 2G structure observed (a) before and (b) after the RH response measurement. (c) a schematic illustration of the humidity response of the 2G structure. The humidity response can be categorized into three regimes; (i) wrinkle regime (response of wrinkles); (ii) complex regime (responses of both wrinkles and microcracks); (iii) self-healing regime (response of microcracks). With increasing RH modulation cycles, the humidity response changes from (i) through (ii) to (iii). Optical microscope images of 1G structure (d) before and (e) after the RH response measurement. The 1G structure (f) can be eliminated at higher relative humidity, to give an almost flat surface (g), and it recovers its original morphology at lower humidity, as shown in (d) and (e).



system enables the formation of hierarchical structures with humidity response (Fig. 1). Using Si alkoxides, such as TEOS, which have exceptionally low reactivities compared with those of alkoxides containing other metal centers<sup>25</sup>, allows precise control of reaction kinetics. Another advantage of the silica–polymer hybrid system is that silica-based materials, such as PDMS, are well known to be environmentally-friendly and relatively stable under severe environments as may be found in device usage. Formation of multilayer structures in the films creates the possibility for wrinkle generation, and therefore, the key to wrinkle formation in this study is appropriate control of polymerization kinetics. We first attempted to use Irgacure 184® as an initiator; however, the rapid polymerization of AM resulted in PAM networks developing throughout the entire film, rather than formation of a multilayered structure, even when the amount of initiator was reduced. The replacement of Irgacure 184® with BDBP retards AM polymerization, and thus the system forms a multilayer. The results shown in Supplementary Figs. S1 and S2 strongly indicate the following wrinkle formation mechanism for bilayer structures: 1) UV irradiation forms a stiff layer, *i.e.*, PAM layer at the top and silica–PVP layer at the bottom; 2) subsequent moderate development of siloxane networks in the bottom layer induces contraction, which creates strain between the layers, and eventually forms wrinkles.

In the present study, three classes of wrinkled structures were obtained, depending on the film thickness: 1) 2G structure, 2) 1G structure + 2G structure (NW structure), and 3) 1G-dominated structure (Fig. 2). As summarized in Fig. 3c, the  $\lambda$  values of the wrinkles, ranging from a few to several tens of micrometres, can be tuned by changing the spinning rate used for the coating operation, *i.e.* the film thickness;  $\lambda$  of a 1G structure is well below 10  $\mu\text{m}$ . Also, the amplitude of the wrinkles changes correspondingly (See Supplementary Fig. S5). Although the formation mechanisms for NW structures have been poorly-understood<sup>22</sup>, the results shown in Fig. 3 and Supplementary Fig. S3 suggest the following plausible mechanism: first, UV induced photopolymerization forms a stiff PAM layer (layer 1) on the film surface, formation of this layer drives counter diffusion of components to form a diffusive layer (layer 2). In parallel with this, evaporation of the solvent leaves behind a relatively soft silica–PVP layer (layer 3). The incorporation of PVP into oxide films has been reported to largely reduce the solvent evaporation<sup>20,26</sup>. Therefore, the evaporation is expected to be much slower in layer 3 than layers 1 and 2. At this stage, the networks of siloxane bonds are weakly-branched and not fully developed in the bottom layers (layers 2 and 3). Subsequent solvent evaporation accelerates the formation of more rigid siloxane networks in layer 2 and induces contraction in this layer. The stress created between layer 1 and layer 2 is first relieved by buckling to form a 1G structure. Whilst the 1G structure is forming, photopolymerization of the stiff surface layer and solvent-evaporation-induced condensation of layer 3 continue. Further contraction of layer 3 accumulates additional strain, which is released by further buckling, resulting in the formation of the 2G structure. Indeed, 1G structure formation, in the present study, is accompanied by trilayer formation; neither the NW nor 1G-dominated structures formed on a bilayer film. This observation supports the structure formation mechanism detailed above.

The 1G structure forms at lower spinning rates, *i.e.*, on thicker films, as shown in Figs. 2 and 3c. The decreased spinning rate, which in turn produces a thicker film, retards evaporation of solvent; the time required for wrinkle formation depends on the film thickness, as explained in the Results section. The 1G structure is also favoured when the reaction is prolonged by decreasing the UV power used to irradiate the films. These results are explained by moderate reaction kinetics ensuring diffusion of components and successful formation of the diffusive intermediate layer (layer 2). Indeed, such concentration gradients of components must occur, because counter diffusion of AM and hydrolyzed TEOS is induced during UV irradiation. The

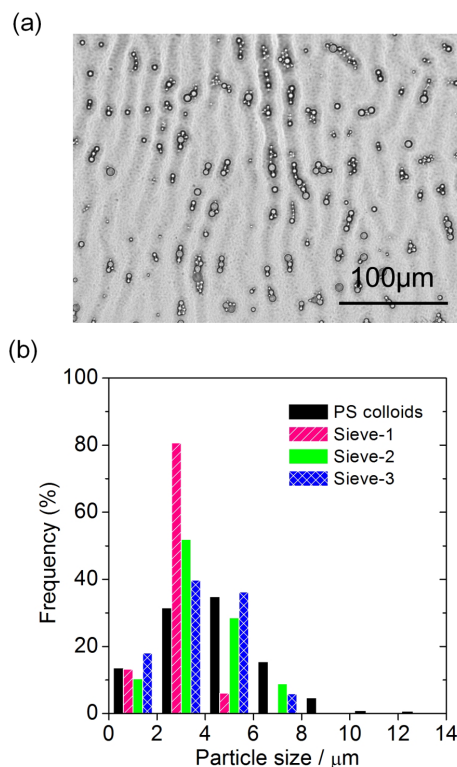


**Figure 6 | NW structures act as an active adsorption surface.** (a) an optical microscope image showing particles captured by wrinkles. The film was coated onto a glass substrate at a spinning rate of 1000 rpm ( $t \sim 12.4 \mu\text{m}$ ) (see Supplementary Fig. S4 for results obtained at other spinning rates). (b) particle size distributions of the original PS colloids and the particles size-selected by wrinkle structures prepared at different spinning rates. Sieve-1: 500 rpm ( $t \sim 23.1 \mu\text{m}$ ); Sieve-2: 1000 rpm ( $t \sim 12.4 \mu\text{m}$ ); Sieve-3: 1500 rpm ( $t \sim 9.5 \mu\text{m}$ ).

penetration depth of irradiated UV light ( $\lambda = 254 \text{ nm}$ ) is 788 nm which is smaller than the thickness of layer 1 (3.68  $\mu\text{m}$ ); this implies diffusion of components during the reaction (see Supplementary Fig. S6).

It is noteworthy that the humidity response of the 1G structure is completely different from that of the 2G structure. As is obvious from Fig. 5 d and e, the 1G structure remained free from micro-cracks, even after repeated RH modulation. This was probably because of the smaller strain accumulated in 1G structures compared to that in 2G structures. Meanwhile, the 1G structure is also humidity responsive and maintains its wrinkled state (See (i) in Fig. 5c) throughout repeated RH modulations. Since the intact 1G structure shows a negative correlation with RH, the stress-accumulation and stress-relief behaviour of the 1G structure is completely opposite to that of the 2G structure, which is in the self-healing regime; for example, under low RH, a stress-accumulated 1G structure and a stress-relieved 2G structure will coexist in the same film. Thus, the NW structure in the self-healing regime offers mutually-opposite responses from two distinct size scales. The coexistence of opposite responses originating from opposite stress-accumulations, as observed in this study, is quite rare amongst previously reported stimuli-responsive materials. These characteristic features will open up the option of independent control of individual structures by external stimuli, which could be exploited in various applications, such as the controlled release of adsorbed particles with different sizes (for example, the particles in Fig. 6), though further modulated control of the response from the 1G structure is required.



## Methods

**Silica–polymer film synthesis.** Tetraethoxysilane (TEOS) was used as the Si source, and acrylamide (AM) as the photomonomer. A mixture of Ethanol (EtOH,  $\geq 99.5\%$ ) and  $\text{H}_2\text{O}$  was used as the solvent. Concentrated nitric acid ( $\text{HNO}_3$ , 60 wt.% in water) was used as a catalyst for hydrolysis and condensation of TEOS. Two types of poly(vinylpyrrolidone) (PVP) with different molecular weights (PVP-K30,  $M_w = 4.0 \times 10^5$  and PVP-K90,  $M_w = 3.6 \times 10^5$ ) were added to control viscosity. 4, 4'-Bis(dimethylamino)benzophenone (BDBP) was used as an initiator for photo-induced polymerization of AM. TEOS was purchased from Shin-Etsu Chemical Co. Ltd., and all other chemicals were obtained from Wako Pure Chemicals Industry Co. Ltd. First, 5.46 g of silica precursor sol was prepared from TEOS, EtOH,  $\text{H}_2\text{O}$ , and  $\text{HNO}_3$  (mole ratio: TEOS:EtOH: $\text{H}_2\text{O}$ : $\text{HNO}_3 = 1:7.85:4.42:1.31$ ) under ice-cooling. Then, the sol was mixed with 7.56 g of AM ethanolic solution (mole ratio: AM:EtOH = 1:1.58) containing 6.95 wt.% of PVP-K30 and 6.95 wt.% of PVP-K90. BDBP (5.24 wt.%) was then added to this mixture, followed by further stirring with ice cooling in the dark. The homogeneous coating solution thus obtained was spin-coated on either soda–lime glass or Si substrates at various spinning rates from 500 to 2000 rpm. Subsequent UV light irradiation (254 nm, intensity  $8.5 \mu\text{W cm}^{-2}$ ) under ambient conditions formed a silica–polymer hybrid film after a period of  $\sim 4$  hours. Some of the UV-cured films formed a dual-periodic structure. In this study, we refer to the smaller structure as the 1G structure (1<sup>st</sup> generation structure), and the larger structure as 2G structure (2<sup>nd</sup> generation structure).

**Structural characterization.** The morphologies of the obtained films were observed using an optical microscope (BX51, OLYMPUS Corp.) and a laser scanning confocal microscope (LSCM) (SFT–3500, Shimadzu Corp.). Two-dimensional optically sliced images obtained with LSCM were stacked and reconstructed into a 3D image. Structural evolution during UV irradiation was observed using a CCD video camera module (SHIGMA KOKI Co. Ltd.). The UV light was irradiated from the film-coated side, and the observation was carried out from the opposite side through a glass substrate. A compositional depth profile of the wrinkled film was obtained using a glow-discharge optical emission spectrometer (GD-OES: GDA750, Rigaku Corp./Spectra Analytik GmbH). The sample film was sputtered in an Ar atmosphere of 250 Pa by applying a radio frequency of 6.78 MHz at a power of 20 W. The diameter of the sputtered craters was approximately 4 mm. Prior to the sample analysis, sol-gel films with known compositions were analyzed and the relative sputtering rates of the respective atoms were calibrated. Fourier transform infrared spectroscopy (FT-IR: ALPHA FT-IR spectrometer, Bruker Optik GmbH) and Ultraviolet-visible spectroscopy (UV-Vis: V-670 spectrophotometer, JASCO Corp.) were employed to analyze the chemical composition of the UV-cured film and to estimate the penetration depth of UV light into the reacting film, respectively.

**Humidity response of silica–polymer film.** *In situ* small angle light scattering (SALS) measurements were carried out on a film placed in a relative humidity (RH) controllable chamber, and the RH response of the surface wrinkles was investigated. The SALS measurement was performed with a 15 mW He-Ne laser (632.8 nm) as a light source, and the first order diffraction from the surface wrinkle pattern was collected on a detector through an aperture and a lens<sup>21</sup>. The first order diffraction efficiency,  $(\eta_{1st}) = (\text{intensity of the first order diffraction ring}) / (\text{intensity of the incident laser light})$ , was used to estimate the change of the amplitude of the wrinkles. The RH in the chamber was first increased from 8% to 60%, and then decreased again to 8%. This modulation of RH was repeated over 50 times to investigate the cycling characteristics of the RH response. The analyzed sample had a 2G structure with  $\lambda = 29.2 \mu\text{m}$ , and the 1st order diffraction appeared at a diffraction angle of  $1.24^\circ$  under ambient atmosphere. Though the diffraction angle could decrease to  $1.21^\circ$  during the measurement because of the increased  $\lambda$  induced by swelling of the bottom layer, the detector could cover the angle range from  $0.95$  to  $1.99^\circ$  and so 1st order diffraction was successfully collected throughout the humidity modulation.

- Kanazawa, H. *et al.* Temperature-responsive chromatography using poly(N-isopropylacrylamide)-modified silica. *Anal. Chem.* **68**, 100–105 (1996).
- Hosoya, K. *et al.* Novel surface-modification techniques for polymer-based separation media stimulus-responsive phenomena based on double polymeric selectors. *J. Chromatogr. A* **1030**, 237–246 (2004).
- Osada, Y. & Gong, J. Stimuli-responsive polymer gels and their application to chemomechanical systems. *Prog. Polym. Sci.* **18**, 187–226 (1993).
- Beebe, D. J. *et al.* Functional hydrogel structures for autonomous flow control inside microfluidic channels. *Nature* **404**, 588–590 (2000).
- De Las Heras Alarcón, C., Pennadam, S. & Alexander, C. Stimuli responsive polymers for biomedical applications. *Chem. Soc. Rev.* **34**, 276–285 (2005).
- Stuart, M. A. C. *et al.* Emerging applications of stimuli-responsive polymer materials. *Nat. Mater.* **9**, 101–113 (2010).
- Sanchez, C., Julián, B., Belleville, P. & Popall, M. Applications of hybrid organic–inorganic nanocomposites. *J. Mater. Chem.* **15**, 3559–3592 (2005).

- Bowden, N., Brittain, S., Evans, A. G., Hutchinson, J. W. & Whitesides, G. M. Spontaneous formation of ordered structures in thin films of metals supported on an elastomeric polymer. *Nature* **393**, 146–149 (1998).
- Bowden, N., Huck, W. T. S., Paul, K. E. & Whitesides, G. M. The controlled formation of ordered, sinusoidal structures by plasma oxidation of an elastomeric polymer. *Appl. Phys. Lett.* **75**, 2557–2559 (1999).
- Müller-Wiegand, M., Georgiev, G. & Oesterschulze, E. Spinodal patterning in organic–inorganic hybrid layer systems. *Appl. Phys. Lett.* **81**, 4940–4942 (2002).
- Chan, E. P., Smith, E. J., Hayward, R. C. & Crosby, A. J. Surface wrinkles for smart adhesion. *Adv. Mater.* **20**, 711–716 (2008).
- Chandra, D. & Crosby, A. J. Self-wrinkling of UV-cured polymer films. *Adv. Mater.* **23**, 3441–3445 (2011).
- Cuvendiren, M., Yang, S. & Burdick, J. A. Swelling-induced surface patterns in hydrogels with gradient crosslinking density. *Adv. Funct. Mater.* **19**, 3038–3045 (2009).
- Cuvendiren, M. & Burdick, J. A., Yang, S. Kinetic study of swelling-induced surface pattern formation and ordering in hydrogel films with depth-wise crosslinking gradient. *Soft Mater.* **6**, 2044–2049 (2010).
- Katzenberg, F. Topographic processing of silicone surfaces. *Surf. Coat. Technol.* **200**, 1097–1100 (2005).
- Volynskii, A. L., Bazhenov, S., Lebedeva, O. V. & Bakeev, N. F. Mechanical buckling instability of thin coatings deposited on soft polymer substrates. *J. Mater. Sci.* **35**, 547–554 (2000).
- Groenewold, J. Wrinkling of plates coupled with soft elastic media. *Phys. A* **298**, 32–45 (2001).
- Stafford, C. M. *et al.* A buckling-based metrology for measuring the elastic moduli of polymeric thin films. *Nat. Mater.* **3**, 545–550 (2004).
- Kim, H. S. & Crosby, A. J. Solvent-responsive surface via wrinkling instability. *Adv. Mater.* **23**, 4188–4192 (2011).
- Takahashi, M. *et al.* Photoinduced formation of wrinkled microstructures with long-range order in thin oxide films. *Adv. Mater.* **19**, 4343–4346 (2007).
- Takahashi, M. *et al.* Photo-fabrication of titania hybrid films with tunable hierarchical structures and stimuli-responsive properties. *Adv. Mater.* **22**, 3303–3306 (2010).
- Efimenko, K. *et al.* Nested self-similar wrinkling patterns in skins. *Nat. Mater.* **4**, 293–297 (2005).
- Cerda, E. & Mahadevan, L. Geometry and physics of wrinkling. *Phys. Rev. Lett.* **90**, 074302-1–074302-4 (2003).
- Kakiuchida, H., Takahashi, M., Tokuda, Y. & Yoko, T. Rewritable holographic structures formed in organic–inorganic hybrid materials by photothermal processing. *Adv. Funct. Mater.* **19**, 2569–2576 (2009).
- Brinker, C. J. & Scherer, G. W. *Sol–Gel Science. The Physics and Chemistry of Sol–Gel Processing*, Academic Press, San Diego, 1990.
- Kozuka, H., Kajimura, M., Hirano, T. & Katayama, K. Crack-free, thick ceramic coating films via non-repetitive dip-coating using polyvinylpyrrolidone as stress-relaxing agent. *J. Sol–Gel Sci. Tech.* **19**, 205–209 (2000).

## Acknowledgments

We acknowledge partially financial support from a Grant-in-Aid for Challenging Exploratory Research (No. 22655071), a Grant-in-Aid for Scientific Research (B) (No. 22360276), and a Grant-in-Aid for Young Scientists (B) (No.24750206) from the Ministry of Education, Culture, Sports, Science and Technology (MEXT), administered by the Japan Society for the Promotion of Science (JSPS). Y. T. is also partially supported financially by a research grant from The Murata Scientific Foundation. Ms. H. Takahara of Rigaku Corp. is acknowledged for her support in performing the GD-OES analysis. We are grateful to Dr. R. Makiura of Osaka Prefecture University for helpful discussions.

## Author contributions

Y.T. and M.T. planned research. K.S. executed the materials synthesis and characterization. K.S. and T.K. performed in-situ SALS analysis. All authors prepared and reviewed the manuscript.

## Additional information

**Supplementary information** accompanies this paper at <http://www.nature.com/scientificreports>

**Competing financial interests:** The authors declare no competing financial interests.

**License:** This work is licensed under a Creative Commons Attribution-NonCommercial-ShareAlike 3.0 Unported License. To view a copy of this license, visit <http://creativecommons.org/licenses/by-nc-sa/3.0/>

**How to cite this article:** Tokudome, Y., Suzuki, K., Kitanaga, T. & Takahashi, M. Hierarchical Nested Wrinkles on Silica–Polymer Hybrid Films: Stimuli-Responsive Micro Periodic Surface Architectures. *Sci. Rep.* **2**, 683; DOI:10.1038/srep00683 (2012).